Nonlinear Dyn
https://doi.org/10.1007/s11071-023-08501-y



ORIGINAL PAPER

# New physical insights in dynamical stabilization: introducing Periodically Oscillating-Diverging Systems (PODS)

**Alvaro A. Grandi** · **Suzie Protière** · **Arnaud Lazarus**

Received: 6 December 2022 / Accepted: 11 April 2023


**Abstract** Dynamical stabilization is the ability of a statically diverging stationary state to gain stability by periodically modulating its physical properties in time. This phenomenon is getting recent interest because it is one of the exploited feature of Floquet engineering that develops new exotic states of matter in the quantum realm. Nowadays, dynamical stabilization is done by applying periodic modulations much faster than the natural diverging time of the Floquet systems, allowing for some effective stationary equations to be used instead of the original dynamical system to rationalize the phenomenon. In this work, by combining theoretical models and precision desktop experiments, we show that it is possible to dynamically stabilize a system, in a "synchronized" fashion, by periodically injecting the right amount of external action in a pulse wave manner. Interestingly, the Initial Value Problem underlying this fundamental stability problem is related to the Boundary Value Problem underlying the determination of bound states and discrete energy levels of a particle in a finite potential well, a well-known problem in quantum mechanics. This analogy offers a universal semi-analytical design tool to dynamically stabilize a mass in a potential energy varying in a square-wave fashion.

**Keywords** Dynamical systems · Time-periodic systems · Stability analysis · Control · Floquet theory

**Supplementary Information** The online version contains supplementary material available at https://doi.org/10.1007/s11071-023-08501-y.

A. A. Grandi · S. Protière · A. Lazarus (✉)
Institut Jean Le Rond d'Alembert, CNRS UMR7190, Sorbonne Université Paris, Paris, France
e-mail: arnaud.lazarus@sorbonne-universite.fr

## 1 Introduction

Floquet engineering is a passive technique that enables to shape the effective potential energy landscape of a physical system by periodically varying its geometrical or mechanical properties in time [1,2]. This technique is widely used in physics because it can cause particles or systems to move to new stable equilibrium configurational states that would otherwise not exist when no periodic modulations are applied. For example, by periodically varying gravitational acceleration through the use of a mechanical shaker, naturally collapsing inverted pendulums can be dynamically stabilized [3,4] and the direction of buoyancy can be inverted so that boats start to float upside-down [5]. This idea of dynamical stabilization also allows to trap naturally diverging charged particles in periodically varying electromagnetic fields [6] which is the key mechanism of mass spectrometers. Using a driving laser with periodic pulses, Floquet engineering is also exploited to generate new electronic properties in a solid, turning insulator into a metal or a metal into a superconductor [7].

The fundamental model to rationalize those dynamical phenomena is the one of a single 1 degree-of-freedom (d.o.f.) mass in a potential energy landscape that is periodically modulated in time [8,9]. Floquet engineering assumes that the time scale of modulation is much shorter than the natural time scales of the moving mass so that averaging techniques and separation of time scales can be used and the concept of a resulting effective potential energy landscape is applicable [10]. In this framework, the principle of dynamical stabilization, firstly rationalized by Kapitza in 1951 [11,12], is that a naturally *diverging* mass in a potential with a negative local curvature can be dynamically stabilized by *periodically* modulating the curvature, as soon as the modulations are fast enough with respect to the diverging speed and the curvature is at least positive, i.e., the mass is *oscillating* in a potential well, for some time over the period.

The stability diagram of the aforementioned 1 d.o.f. Periodically Oscillating-Diverging System (P.O.D.S.) is easy to compute and consists of alternating stability and instability tongues in the modulation parameter space. Kapitza's averaging techniques allow to rationalize one asymptotic limit of the first stability tongue of a P.O.D.S., but the rest of the stability diagram, where the diverging and the modulation time scales are of same order of magnitude, has been overlooked, especially from a physical point of view. We believe it is important to gain physical insights in this regime that we coin "synchronized stabilization" since, not only it represents an important theoretical asymptotic limit that could be of practical importance for Floquet engineering, but it also embraces a fundamental problem in physics, that is not addressed with Kapitza's approach: what is the minimal amount of external action (external potential energy added over time) periodically needed to dynamically stabilize a mass. In this paper, we answer those questions on a 1 degree of freedom P.O.D.S. model with a square wave modulation function (in this case, the stability diagram is analytically defined) that we study both experimentally and numerically.

When trying to dynamically stabilize the mass but spending most of the period in a diverging state, we found that stabilization still exists but in discrete and narrow regions of the modulation parameter space which correspond to the tips of the stability tongues of our P.O.D.S. In this asymptotic limit, it means only a discrete set of square-wave modulation functions exists for which the oscillations of the perturbed mass would remain bounded about its equilibrium position. Moreover, after proper scaling, those marginally stable oscillations can be described by a single periodic carrier function whose modal shape depends on the order of the stability tongue we consider. Interestingly, the location of the tips and the shape of the periodic carrier can be pseudo-analytically obtained by solving an eigenvalue problem with varying coefficients in an infinitely large elementary time-cell (mathematically analog to the one of a particle in a finite potential well which is a famous problem in quantum physics [13]) instead of classically solving the original initial value problem. Finally, by re-introducing the diverging period, it turns out the "quantum" analog problem leads to master curves in the whole modulation parameter space that are always located in the stability tongues of the P.O.D.S. This offers design opportunities that we validate experimentally with the dynamical stabilization of an electromagnetic pendulum.

In Sect. 2, we introduce the P.O.D.S. model of a 1 d.o.f. mass in a potential energy landscape that vary periodically in time in a square wave fashion, altogether with its model experiment that is the dynamical stabilization of an electromagnetic inverted pendulum developed in our laboratory. In Sect. 3, thanks to numerical experiments, we rationalize the physics of the dynamically stabilized mass for modulation functions located at the tips of the stability tongues. Based on the results of Sect. 3, we propose in Sect. 4 a pseudo-analytical method to derive master curves that belong to the stability tongues whatever the chosen modulation parameters of the P.O.D.S. Thanks to this property, we show that we can use those pseudo-analytical master curves to easily find the modulation parameters required to dynamically stabilize the aforementioned electromagnetic inverted pendulum.

## 2 The square-wave P.O.D.S.

### 2.1 Definition of the concept

Let us consider a mass parameterized by the generalized coordinate $q(t)$ and its derivative with respect to time $\dot{q}(t)$. For simplicity, we can say $q(t)$ is dimensionless (it could be an angle for example). We then assume that the kinetic energy $\mathcal{T}(\dot{q})$ of the particle is





Journal: 11071 MS: 8501 TYPESET DISK LE CP Disp.:2023/5/16 Pages: 19 Layout: Medium

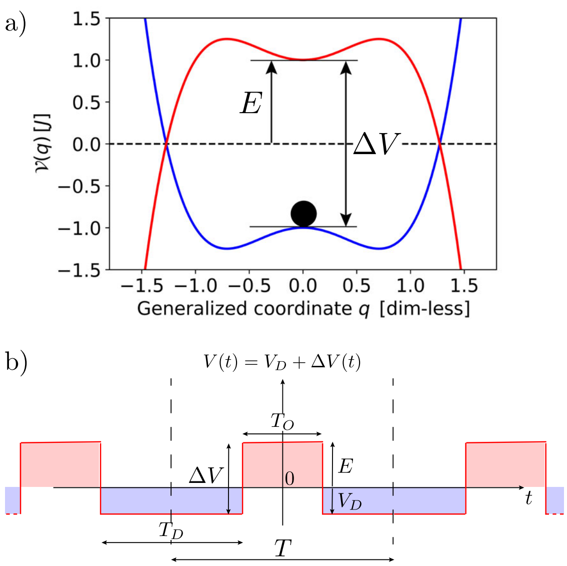


**Fig. 1** One degree of freedom model of a Periodically Oscillating-Diverging System (P.O.D.S.) with a square wave periodic potential energy $\mathcal{V}(q, t) = V(t) \times (1 + q^2 - q^4)$. **a** Mass in a potential energy landscape that periodically "jumps" between $\mathcal{V}(q) = V_\mathrm{D} \times (1 + q^2 - q^4)$ in blue line and $\mathcal{V}(q) = E \times (1+q^2-q^4)$ in red line with $E = V_\mathrm{D}+\Delta V$. Here, $V_\mathrm{D} = -1$ and $\Delta V = 2$. **b** Square wave modulation function $V(t)$

in the classic quadratic form:

$$\mathcal{T}(\dot{q}) = \frac{1}{2} I \dot{q}^2 \tag{1}$$

with $I$ the moment of inertia of the mass. Let us also assume the mass is in a potential energy (adding a constant does not change the physics of the mass)

$$\mathcal{V}(q, t) = V(t) \times (1 + q^2 - q^4) \quad (+\mathrm{Cste}) \tag{2}$$

where $V(t) = V_\mathrm{D} + \Delta V(t)$ is a square function illustrated in Fig. 1b, $V_\mathrm{D} < 0$ and $\Delta V(t) = \Delta V(t + T)$ with $T = T_\mathrm{O} + T_\mathrm{D}$ the period. During $T_\mathrm{D}$, the "diverging time", we have $\Delta V(t) = 0$ and the potential looks like the one in blue line in Fig. 1a, whereas during $T_\mathrm{O}$, the "oscillating time", $\Delta V(t) = \Delta V$ and the potential corresponds to the red line in Fig. 1a. It is clear from Fig. 1 that in the static case $\Delta V(t) = \Delta V$ for all $t$, the mass would be stable about the equilibrium $q = 0$ only if $\Delta V > |V_\mathrm{D}|$, i.e., the mass is in a potential energy with a local positive curvature about $q = 0$. But in the dynamical case $\Delta V(t) = \Delta V(t + T)$, it should be possible to periodically have moments when $\Delta V < |V_\mathrm{D}|$ and still be locally stable. The question of stability then becomes intricate, and one needs to start looking at the equation of motion of the mass.

To predict the motion of the mass parameterized by $q(t)$ and $\dot{q}(t)$ in such a potential energy, one can derive the Hamilton equations. To do so, we introduce the generalized impulsion $p(t) = \partial\mathcal{L}(q, \dot{q}, t)/\partial\dot{q} = I\dot{q}$ where

$$\begin{aligned}\mathcal{L}(q, \dot{q}, t) &= \mathcal{T}(\dot{q}) - \mathcal{V}(q, t)\\ &= \frac{1}{2} I \dot{q}^2 - (V_\mathrm{D} + \Delta V(t))(1 + q^2 - q^4)\end{aligned} \tag{3}$$

is the Lagrangian of the dynamical system. Introducing the time-dependent Hamiltonian

$$\begin{aligned}\mathcal{H}(q, p, t) &= p\dot{q} - \mathcal{L}(q, \dot{q}, t)\\ &= \frac{1}{2} I \dot{q}^2 + (V_\mathrm{D} + \Delta V(t))(1 + q^2 - q^4)\end{aligned} \tag{4}$$

one can derive the nonlinear equations of motion

$$\begin{aligned}\begin{Bmatrix} \dot{q(t)} \\ \dot{p(t)} \end{Bmatrix} &= \begin{Bmatrix} \frac{\partial\mathcal{H}}{\partial p} \\ -\frac{\partial\mathcal{H}}{\partial q} \end{Bmatrix}\\ &= \begin{Bmatrix} p/I \\ -(V_\mathrm{D} + \Delta V(t))(2q - 4q^3) \end{Bmatrix}\end{aligned} \tag{5}$$

The trivial fixed point $(q^*, p^*) = (0, 0)$ is a solution of the nonlinear equations of motion whatever the physical parameters of the system and the linearized equation of motion about $(q^*, p^*) = (0, 0)$ reads simply

$$\begin{Bmatrix} \dot{q(t)} \\ \dot{p(t)} \end{Bmatrix} = \begin{bmatrix} 0 & 1/I \\ -2(V_\mathrm{D} + \Delta V(t)) & 0 \end{bmatrix} \begin{Bmatrix} q(t) \\ p(t) \end{Bmatrix} \tag{6}$$

which can be rewritten in the form of a second-order linear differential equation whose evolution function varies, depending on when we are during a period

$$\begin{cases} \ddot{q}(t) + \frac{2}{I}(V_\mathrm{D} + \Delta V)q(t) = 0 & \text{during } T_\mathrm{O} \\ \ddot{q}(t) + \frac{2}{I} V_\mathrm{D} q(t) = 0 & \text{during} T_\mathrm{D} \end{cases} \tag{7}$$

According to Lyapunov's definition and introducing the state vector $\mathbf{X}(t) = \{q(t), p(t)\}^\mathrm{T}$, we can assess the mass is dynamically stable (or Lyapunov stable) about $\mathbf{X}^* = \{q^*, p^*\}^\mathrm{T} = \{0, 0\}^\mathrm{T}$ if it exists $\delta(\varepsilon) > 0$ such that, if $\|\mathbf{X}(0) - \mathbf{X}^*\| < \varepsilon$, we have $\|\mathbf{X}(t) - \mathbf{X}^*\| < \delta$ for all time. If $\|\mathbf{X}(t) - \mathbf{X}^*\| \to 0$ for $t \to \infty$, the fixed point is called asymptotically stable, and if $\|\mathbf{X}(t) - \mathbf{X}^*\|$ is finite but bounded, $\mathbf{X}^* = \{q^*, p^*\}^\mathrm{T} = \{0, 0\}^\mathrm{T}$ is neutrally stable.





Journal: **11071** MS: **8501** TYPESET DISK LE CP Disp.:**2023/5/16** Pages: **19** Layout: **Medium**

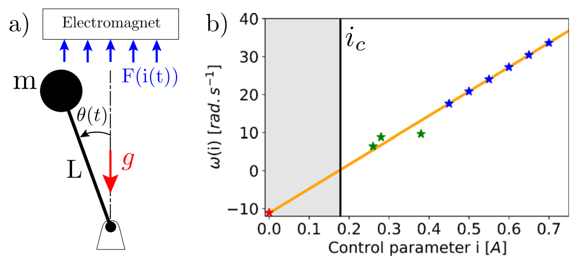


**Fig. 2** Characterization of the experimental P.O.D.S. **a** Sketch of the experimental setup: an inverted pendulum in a symmetric electromagnetic field controlled by the electrical current $i(t)$. **b** Natural time scale $\omega(i)$ of the transverse response of the upright pendulum when subjected to a perturbation for various values of the control parameter $i$ (a minus sign means a characteristic diverging time when a positive $\omega(i)$ corresponds to an angular frequency of the oscillatory motion)

For practical purposes, one can first study the perturbed motion solution of the linearized equations (6) to see for which parameters $V_\mathrm{D}$, $\Delta V$, $T_\mathrm{O}$ and $T_\mathrm{D}$ it exists a basin of attraction of initial conditions in phase space for which the mass will be dynamically stable. An analysis of the nonlinear equations of motion Eq. (5) can then specify the size of this basin of attraction. Because (6) is a set of linear first-order Ordinary Differential Equation (ODE) with periodic coefficient, we can apply Floquet theory to assess the linear stability of the mass. To get better physical insights in the behavior of the aforementioned P.O.D.S. concept, we built an experimental model whose dynamical stability can be described by Eq. (5)–(7).

### 2.2 Experimental PODS: the dynamic stabilization of an inverted pendulum

The 1 degree-of-freedom P.O.D.S. we built in the laboratory is an electromagnetic inverted pendulum (Fig. 2a). It consists of a metallic marble of mass $m = 28$ g that is attached to a plexiglass rod of length $L = 6.2$ cm and mass $m_\mathrm{rod} = 1.5$ g (we neglect the mass of the rod in our calculations of moment of inertia $I$). The rod is then constrained to rotate only in one plane as shown with the picture of the experimental setup in Fig. 12 of Appendix 1. Finally, the mass is symmetrically placed below an electromagnet. When some electrical current $i$ passes through the electromagnet, the latter can attract the metallic bob of the pendulum thanks to electromagnetic forces $F(i)$ in the opposite direction of weight $mg$ where $g = 9.81$ m/s$^2$ is the gravitational acceleration. The motion of the electromagnetic pendulum, that is constrained to move in a plane, is fully parameterized by the angle $\theta(t)$ between the vertical axis and the almost weightless rigid bar.

The zero-order property of a P.O.D.S. like the one depicted in Fig. 1 is the symmetry of the potential energy landscape with respect to the generalized coordinate $q(t)$ parameterizing the mass. This is the case with the electromagnetic pendulum of Fig. 2a since the geometry, electromagnetic forces $F(i)$ and weight $mg$ are all symmetric with respect to the angle $\theta(t) = q(t)$. A direct consequence is that the upright vertical position of the mass $\theta(t) = 0$ is an equilibrium configuration whatever the loading parameter $F(i)$.

The first-order property of a P.O.D.S. is to periodically vary between a negative and positive local curvature of the potential about the equilibrium position $q(t) = 0$. This is indeed a property of the electromagnetic pendulum that is illustrated in Fig. 2b which shows the evolution of the natural time scale of the perturbed pendulum about its upright equilibrium position for various value of the control parameter $i$. When $i = 0$, the electromagnet is OFF and when one initially brings the pendulum upright, the mass is exponentially diverging from the equilibrium $\theta(t) = 0$ with a typical time scale $1/\omega(0) = 0.09$ s (red star, Fig. 2b where we put a minus sign for $\omega(0)$ to highlight that the mass is diverging) that is very close to the theoretical value $\sqrt{L/g} = 0.08$ s. Above a critical current $i_c \approx 0.17$ A, the upright equilibrium position starts to be stable. From $i_c$ to $i \approx 0.4$ A, the mass is neutrally stable and although the perturbed pendulum oscillates back to $\theta(t) \approx 0$, it is difficult to properly define a time scale for the oscillations (green stars, Fig. 2b). Above $i \approx 0.4$ A, the perturbed pendulum performs damped oscillations before coming back to $\theta(t) = 0$, the angular frequency $\omega(i)$ is reproducibly measurable blue stars, Fig. 2b and fairly independent on the strength of the initial perturbations, *i.e.*, the electromagnetic forces $F(i)$ appear constant in the vicinity of the mass.

An experimental square-wave P.O.D.S. is obtained by periodically varying the electrical current $i(t)$ between $i = 0$ A during $T_\mathrm{D}$ seconds and $i = 0.48$ A during $T_\mathrm{O}$ seconds. During a period $T = T_\mathrm{O} + T_\mathrm{D}$, the mass is oscillating around $\theta(t) = 0$ during $T_\mathrm{O}$ and diverging from $\theta(t) = 0$ during $T_\mathrm{D}$, which is indeed what is qualitatively model by a P.O.D.S. (Fig. 1). The experimental stability diagram of the upright equilibrium position $\theta(t)$ as a function of $T_\mathrm{O}$ and $T_\mathrm{D}$ is shown





Journal: **11071** MS: **8501** TYPESET DISK LE CP Disp.:**2023/5/16** Pages: **19** Layout: **Medium**

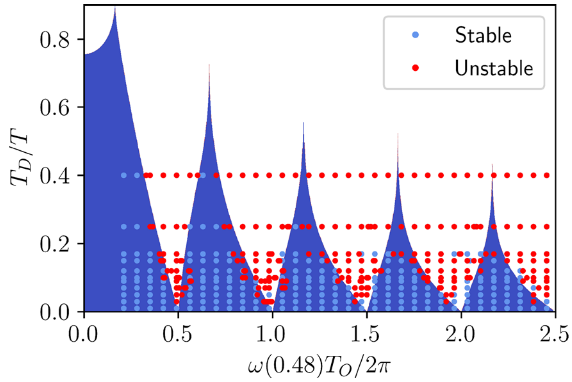


**Fig. 3** Numerical and experimental stability diagram of the upright vertical pendulum when the current is modulated with a square-wave $T$-periodic function: $i = 0$ during $T_\mathrm{D}$ and $i = 0.48$ A during $T_\mathrm{O}$ with $T = T_\mathrm{O} + T_\mathrm{D}$. Blue regions represent dynamically stable $(T_\mathrm{O}, T_\mathrm{D})$ when white regions represent unstable ones. Blue and red dots represent stable and unstable experimental data points, respectively

in blue and red dots in Fig. 3. Unlike the classic Kapitza limit where $T \ll 2\pi/(\omega(0), \omega(0.48))$, we focus on time modulation parameters that are of same order of magnitude than the natural time scales and studied how stabilization behaves when increasing $T_\mathrm{D}/T$. For each data point, our protocol was to first turn the electromagnet ON for 5 s to asymptotically stabilize the inverted pendulum at $\theta(t) = 0$ and then, OFF for 250 ms to perturb the mass before applying the square-wave modulation $i(t)$. If for a modulation function $(T_\mathrm{O}, T_\mathrm{D})$ the initial perturbation is still not amplified after 20 periods, we call it dynamically stable (blue dots). We call it unstable and put a red dot otherwise. In this case, the pendulum often falls or sometimes does some strong oscillations.

The dynamical stability of the aforementioned experimental square-wave P.O.D.S can be rationalized at first order by the linear equations of motion Eq. (7) where the generalized coordinate $q(t)$ is the angle $\theta(t)$ and $I = mL^2 = 1.076 \times 10^{-4}$ kg.m$^2$. During $T_\mathrm{D}$, $i = 0$ A and the diverging mass of the upright inverted pendulum is governed by $\ddot{\theta}(t) - \omega(0)^2\theta(t) = 0$ with $\omega(0) = -11.1$ rad/s as shown in Fig. 2b (see Appendix 1 and movie 1 in [14]). By identification, it comes $V_\mathrm{D} = -\frac{1}{2}I\omega(0)^2 = -1.04$ mJ in Eq. (7). During $T_\mathrm{O}$, $i = 0.48$ A and the perturbed upright pendulum is doing damped oscillations about $\theta(t) = 0$ (see Appendix 1 and movie 2 in [14]). Because we consider $T_\mathrm{O}$ that are relatively small as compared to the damping time scale, the perturbed oscillations can be fairly modeled by the undamped linearized equation $\ddot{\theta}(t) + \omega(0.48)^2\theta(t) = 0$ with $\omega(0.48) = 19.5$ rad/s as inferred from Fig. 2b. By identification, it comes $E = V_\mathrm{D} + \Delta V = \frac{1}{2}I\omega(0.48)^2 = 3.24$ mJ in Eq. (7) so that $\Delta V = 4.28$ mJ. We recall the solution of Eq. (7) can be sought in the Floquet form $\theta(t) = \Psi(t)e^{st} + \bar{\Psi}(t)e^{-st}$ where $\Psi(t) = \Psi(t + T)$ is a $T$-periodic complex eigenfunction and $s$ is a complex eigenvalue called the Floquet exponent [8,15,16]. In the case of a square-wave modulation function, Eq. (7) is called the Meissner equation and the Floquet exponent can be analytically solved [9,17,18]. The blue color regions with $max(\Re(\pm s)) = 0$ in Fig. 3 indicate quasi-periodic oscillating solutions $\theta(t)$ about $\theta(t) = 0$, i.e., a neutrally stable mass when the white regions where $max(\Re(\pm s)) > 0$ point out to infinitely amplified response, i.e., a mass that should dynamically repel from $\theta(t) = 0$ whatever the initial conditions.

Figure 3 shows a remarkable agreement between experimental and numerical results, without fitting parameters. We easily recognize the white parametric instability tongues typical of Floquet systems like P.O.D.S. Those tongues of parametric pumping appear, for $T_\mathrm{D} \to 0$, at particular ratios between the period of modulation $T_\mathrm{O} \approx T$ and the natural period of the system $2\pi/\omega(0.48)$, following $kT_\mathrm{O}/(4\pi/\omega(0.48))$ where $k$ is a positive integer value that represents the number of the tongue. Interestingly, it is easy to observe highly sub-harmonic instability tongues (tongues with large $k$) using a P.O.D.S., whereas it is well known that triggering parametric pumping above $k = 1$ is usually complicated in macroscopic Floquet systems where the modulation of local curvature of potential energy is limited and dissipation is intrinsically important [9]. In this paper, we are not interested in the classic Kapitza limit $T_\mathrm{O} \ll 2\pi/\omega(0.48)$ (very left part of Fig. 3), but rather in the blue stability "tongues" that verify $T_\mathrm{O} \approx 2\pi/\omega(0.48)$. Moreover, we think the limit $T_\mathrm{D} \to T$, i.e., the tips of the stability tongues are of fundamental interest because (i) they are the counterpart of the tips of the instability tongues and unlike them, they remain even in the presence of dissipation (see Appendix 2), (ii) they correspond to the periodic modulation functions with minimal input action $\int \Delta V(t)\mathrm{d}t$ to stabilize a naturally diverging system. In the next section, we explore the tips of the stabilization tongues numerically as they are impossible to reach experimentally using the macroscopic setup presented here.





Journal: 11071 MS: 8501 TYPESET DISK LE CP Disp.:2023/5/16 Pages: 19 Layout: Medium

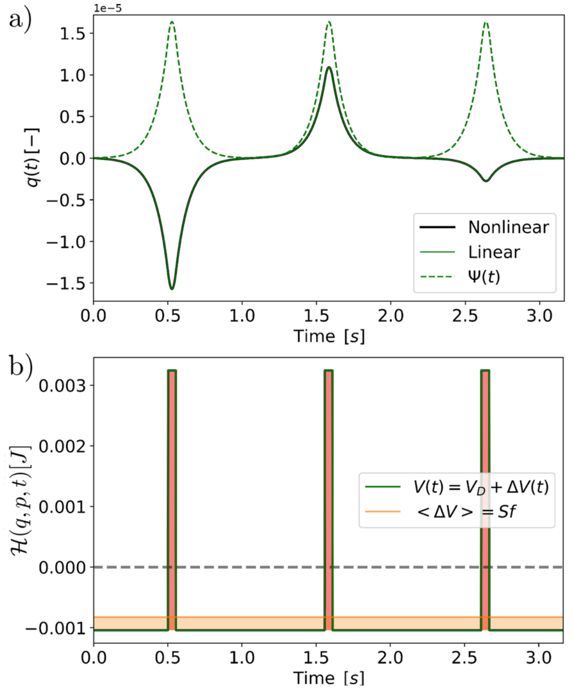


**Fig. 4** Numerical response at the tip of the first stability tongue of Fig. 3 for $T_{\mathrm{O}} = 0.052794$ s and $T_{\mathrm{D}}/T = 0.95$. **a** First three periods of the neutrally stable generalized coordinate $q(t)$ for $q(0) = 0.1 \times 10^{-10}$ and $\dot{q}(0) = -0.2 \times 10^{-10}$ s$^{-1}$. Nonlinear and linear responses are in black and green full line, respectively. The dotted green lines are the Floquet eigenfunctions of the linear response. **b** Hamiltonian of the nonlinear response and modulated function $V(t)$. The average input potential $\langle \Delta V \rangle$ is shown in orange

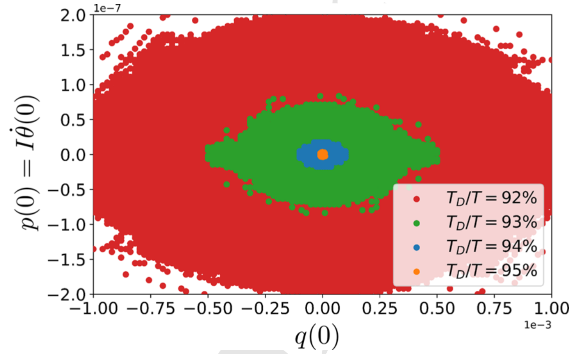


**Fig. 5** Basin of attraction of the fixed point $(q^*, p^*) = (0, 0)$ showing the initial conditions $(q(0), p(0))$ for which the nonlinear response of Eq. (5) is neutrally stable. We place ourselves at the tip of the first stability tongue of Fig. 3 for $T_{\mathrm{O}} = 0.052794$ s

## 3 Numerical investigation of the tip of the stability tongues

In this section, we systematically study the numerical response at the tip of the stability tongues (for practical purposes, we increase $T_{\mathrm{D}}/T$ towards unity, i.e., the Dirac comb scenario, up to the limit of the computational accuracy) in order to rationalize this asymptotic limit.

### 3.1 Synchronized dynamical stabilization

We first show in Fig. 4 an archetypal example of the numerical response of the nonlinear equation of motion (5) at the tip of the first stability tongue of Fig. 3 for $T_{\mathrm{O}} = 0.052794$ s and $T_{\mathrm{D}}/T = 0.95$. Figure 4a shows the evolution of a neutrally stable generalized coordinate $q(t)$ over three period for $q(0) = 0.1 \times 10^{-10}$ and $\dot{q}(0) = -0.2 \times 10^{-10}$ s$^{-1}$ when Fig. 4b shows the evolution of the associated Hamiltonian $\mathcal{H}(q, p, t) = \frac{1}{2} I \dot{q}^2 + (V_{\mathrm{D}} + \Delta V(t))(1 + q^2 - q^4)$ as a function of time as well as the evolution of the square-wave modulation function $V(t) = V_{\mathrm{D}} + \Delta V(t)$ in green line. When approaching the tip of the stability tongue, the basin of attraction drastically shrinks about the equilibrium point $(q^*, p^*) = (0, 0)$ as shown in the phase space of Fig. 5 for the first stability tongue for $T_{\mathrm{O}} = 0.052794$ s. As a consequence, the generalized coordinate $q(t)$ and impulsion $p(t)$ start to be small with respect to $V(t)$ and the Hamiltonian starts to be independent on them such that $\mathcal{H}(q, p, t) \approx \mathcal{H}(t) \approx V(t) = V_{\mathrm{D}} + \Delta V(t)$ where $V(t)$ approaches a Dirac comb when $T_{\mathrm{D}}/T \rightarrow 1$. Another consequence of the initial input energy having to be very small for the mass to be stabilized at the tip of the tongues is that all the neutrally stable responses can be predicted by the linearized Eqs. (6)–(7), as illustrated in Fig. 4a (black and green curves perfectly overlap). According to Floquet theory, it means the oscillatory motion can actually be decomposed in the Floquet form [15], $\theta(t) = \Psi(t)e^{j\Im(s)t} + \bar{\Psi}(t)e^{-j\Im(s)t}$ (since the response is stable, we have $\Re(s) = 0$), where the carrier eigenfunction $\Psi(t) = \Psi(t + T)$ is a $T$-periodic function that is shown in green dotted line in Fig. 4a.

From Figs. 4 and 5, the dynamical stabilization at the tip of the stability tongues can be physically understood by a process that repeats on each period. When $V(t) < 0$ during $T_{\mathrm{D}}/2$, the local curvature of the potential energy is negative and the mass diverges. Then, $V(t)$ becomes positive during $T_{\mathrm{O}}$ and so is the local curvature so that the mass is oscillating. The duration $T_O$ and the value of input potential energy $\Delta V$ are such that, at the moment $V(t)$ becomes negative again, the state of the mass $(q(t), \dot{q}(t))$ is almost the time reversal of the state of this mass $T_O$ seconds ago. As a consequence, when $V(t)$ becomes negative again during $T_D/2$, the motion of the mass decays up to a state $(q(t), \dot{q}(t))$ very close to the one we had $T$ seconds ago. In fine, the modulation function $V(t)$ is such, that the system almost loses its memory after each period and as a consequence, the mass periodically repeats the same motion, albeit with a different amplitude reminiscent of the quasi-periodic nature of the motion. Since in Figs. 4 and 5 we are at the tip of the first stability tongue, the mass has the time to do only one oscillation during $T_O$, i.e., $\dot{q}(t)$ is changing sign only once. Because of this particular physical behavior at the tip of the stability tongues and to contrast with the classic Kapitza stabilization, we coin this phenomenon **synchronized dynamical stabilization**. An interesting property of this synchronized stabilization is shown in Fig. 4b in orange line where we represent the average input potential energy $< \Delta V >= S \times f = (\Delta V \times T_O) \times (1/T)$ where $S$ is the input elementary action and $f$ is the frequency of modulation. When in static, i.e., for $\Delta V(t) = \Delta V$ for all $t$, one needs $\Delta V > |V_D| = 1.04$ mJ to stabilize the naturally diverging system, here one needs in average only $< \Delta V >= 0.213$ mJ to dynamically stabilize the mass. In theory, it seems there is no reason one cannot aim for smaller $< \Delta V >$, at the cost of an even smaller basin of attraction and a tip of stability tongue with a smaller width.

The width of the tip of the stability tongues starts to shrink drastically as $T_D \to T$, nevertheless this width will ever exist in the Meissner equation of motion (7). Figure 6 illustrates what is going on when one navigates in the tip of a stability tongue. Figure 6a, b shows the influence of a perturbation on oscillating time $T_O$ (here, we add 1 $\mu s$) and input energy $\Delta V$ (we add 10 nJ), respectively, on the response of Fig. 4a. We see that the qualitative shape of the neutrally stable responses, that we can decompose in the Floquet form $\theta(t) = \Psi(t)e^{j\Im(s)t} + \bar{\Psi}(t)e^{-j\Im(s)t}$, is still a successive repetition of a scaled version of a similar Floquet eigenfunction $\Psi(t)$, although the scaling on each successive periods is chronologically different. This can be understood because, when moving in the tip of a stability tongue, the imaginary part of the Floquet exponent $\Im(s)$, which is responsible for the modulation of $\Psi(t)$

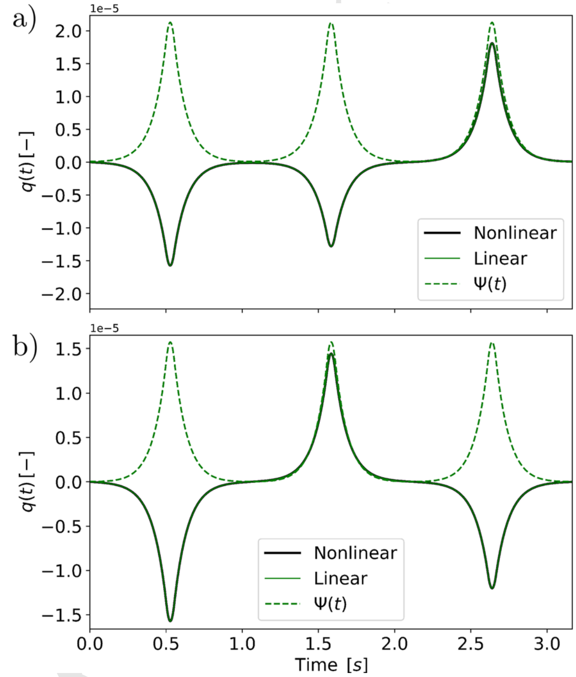


**Fig. 6** Influence of a perturbation in time or energy on the time evolution of the neutrally stable response of Fig. 4. **a** Perturbation of 1 µs on the oscillating time $T_O$. **b** Perturbation of 10 nJ on the input energy $\Delta V$

between each period, is strongly varying between 0 and $\pi/T$. On the contrary, the periodic eigenfunction $\Psi(t)$ remains the same.

### 3.2 From an initial to a boundary value problem

The qualitative behavior highlighted in the previous section suggests that we work in a fix elementary time cell instead of the classic dynamical vision that consists in looking at the state variables as time is passing. This is what we do in Fig. 7a where we have superposed in color lines the 20 first periods of the various neutrally stable $q(t)$ of Figs. 4 and 6 on a single elementary cell between $-T/2$ and $T/2$ (we recall the stability of the mass is not altered by a phase difference of the modulation function $V(t)$). We also report in black line on that figure the periodic eigenfunctions $\Psi(t)$ of Fig. 6a that we recall is almost not influenced by where we are located in the tip of the stability tongue. We see that all the responses are similar but differ from a scaling factor so that, if we were to represent an infinity of periods of a given point at the tip of the stability tongue, the



Journal: 11071 MS: 8501 TYPESET DISK LE CP Disp.:2023/5/16 Pages: 19 Layout: Medium

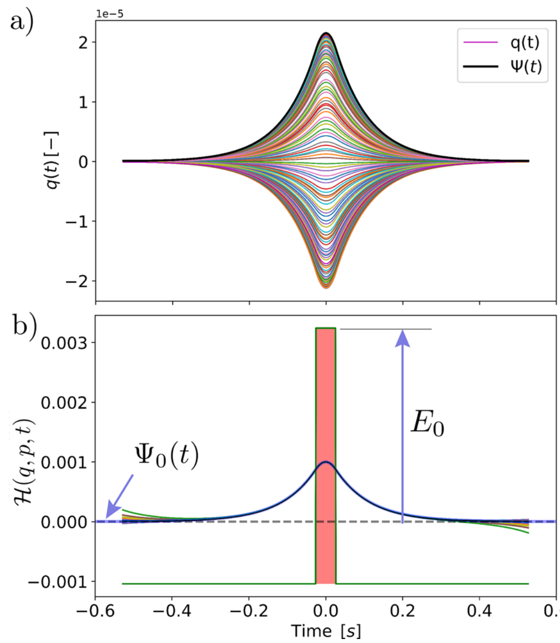


**Fig. 7** Numerical response of Figs. 4, 5, 6 and 7 at the tip of the first stability tongue for $T_\mathrm{O} = 0.052794$ s and $T_\mathrm{D}/T = 0.95$ visualized in the elementary time cell $-T/2 < t < T/2$. **a** Evolution of the generalized coordinate $q(t)$ and Floquet eigenfunction $\Psi(t)$. **b** Collapse of the trajectories $q(t)$ of **a** on the Floquet eigenfunction $\Psi(t)$ and evolution of the associated modulation function $V(t)$ (equivalent to $\mathcal{H}(q, p, t)$). The eigenfunction $\Psi_0(t)$ and eigenvalue $E_0$ of Eq. (9) are reported on the figure

trajectories will completely fill the area between $\Psi(t)$ and $-\Psi(t)$. By renormalizing all the trajectories $q(t)$ in the elementary periodic cell by the correct scaling factor, one can collapse all the curves on the Floquet eigenfunction $\Psi(t)$ as shown in Fig. 7b. In order to plot $\Psi(t)$ on the same figure as the Hamiltonian $\mathcal{H}(q, p, t)$, which we recall tends to the modulation function $V(t)$, we chose a normalization factor so that the maximum of $\Psi(t)$ is 0.001. The few residues that appear close to the boundaries $-T/2$ and $T/2$ correspond to the trajectories whose extremum is very close to zero and exist because we are not numerically at the very end of the tip ($T_\mathrm{D}/T = 0.95$).

So, at the tip of the stability tongue, synchronized dynamical stabilization can be characterized by a Floquet eigenfunction $\Psi(t)$ that is the carrier of the modulated neutrally stable response $q(t)$ and an associated modulation function $V(t)$ (that turns out to be also the energy of the mass's motion) as shown in Fig. 7b. With this approach in the elementary periodic cell $-T/2$ and $T/2$, we lost information about the actual response $q(t)$ that is a sequence of scaled $\Psi(t)$ periods after periods and we lost track of the width of the tip of the stability region or the basin of attraction, but we will be able to derive a boundary problem to analytically predict the triplet $(T_\mathrm{O}, \Delta V, E)$ and $\Psi(t)$ that stabilize the mass for $T_\mathrm{O} \ll T$.

The first step for this is to note that, since $E = V_\mathrm{D} + \Delta V$, the linearized equation of motion (7) can be recast in the form of a linear eigenvalue problem with a variable coefficient in the elementary periodic cell

$$\begin{cases} \left(-\dfrac{I}{2}\dfrac{\mathrm{d}^2}{\mathrm{d}t^2} + 0\right)\Psi(t) = E\Psi(t) & \text{for } |t| < \dfrac{T_\mathrm{O}}{2} \\ \left(-\dfrac{I}{2}\dfrac{\mathrm{d}^2}{\mathrm{d}t^2} + \Delta V\right)\Psi(t) = E\Psi(t) & \text{for } \dfrac{T_\mathrm{O}}{2} < |t| < \dfrac{T}{2} \end{cases} \tag{8}$$

where because of the normalization of $\Psi(t)$ and its compact form on $[-T/2, T/2]$, we will assume the boundary conditions $\Psi(-T/2) = \Psi(T/2) = 0$. As we go closer to the tip of the stability tongue, the compacity of $\Psi(t)$ is ever more pronounced and $T \gg T_\mathrm{O}$ so that we are encouraged to get rid of the diverging modulating time and write equation (8) on an infinite elementary time cell

$$\left(-\frac{I}{2}\frac{\mathrm{d}^2}{\mathrm{d}t^2} + \mathcal{U}(t)\right)\Psi(t) = E\Psi(t) \tag{9}$$

$$\text{with} \quad \begin{cases} \mathcal{U}(t) = 0 & \text{for } |t| < \dfrac{T_\mathrm{O}}{2} \\ \mathcal{U}(t) = \Delta V & \text{for } |t| > \dfrac{T_\mathrm{O}}{2} \end{cases}$$

$$\text{and} \quad \Psi(-\infty) = \Psi(+\infty) = 0.$$

Doing so, the variable $T$ (or $T_\mathrm{D}$) is no more visible in Eq. (9), but the latter is now a famous Sturm–Liouville problem that can be analytically solved (Appendix 3 describes the theoretical process to compute $E$ and $\Psi(t)$). In fact, Eq. (9) is the sort of mathematical equation that underly the quantum eigenvalue problem that consists in finding the energy levels and stationary wave functions of a particle confined in a finite potential well [13]. To confirm that this boundary value problem is the one that relates $T_\mathrm{O}$, $\Delta V$, $E$ and $\Psi(t)$ close to the tip of the stability tongue in the infinite elementary time cell, we apply it to the numerical data we showed in Fig. 7. Taking $T_\mathrm{O} = 0.052794$ s and $\Delta V = 4.28$ mJ (we fix the elementary action $S = T_\mathrm{O} \times \Delta V$ shown in red in Fig. 7), we find an eigenvalue $E_0 = 3.24$ mJ and an eigenvector $\Psi_0(t)$ that matches the ones we found in





Journal: 11071 MS: 8501 TYPESET DISK LE CP Disp.:2023/5/16 Pages: 19 Layout: Medium

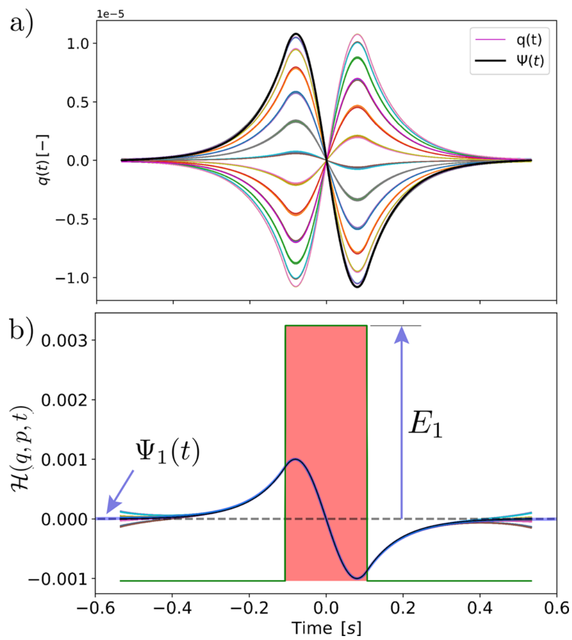


**Fig. 8** Numerical response at the tip of the second stability tongue of Fig. 3 for $T_\mathrm{O} = 0.21365$ s and $T_\mathrm{D}/T = 0.8$ visualized in the elementary time cell $-T/2 < t < T/2$. **a** Evolution of the generalized coordinate $q(t)$ and Floquet eigenfunction $\Psi(t)$. **b** Collapse of the trajectories $q(t)$ of **a** on the Floquet eigenfunction $\Psi(t)$ and evolution of the associated modulation function $V(t)$ (equivalent to $\mathcal{H}(q, p, t)$). The eigenfunction $\Psi_1(t)$ and eigenvalue $E_1$ of Eq. (9) are reported on the figure

Fig. 7b. Note that the eigenfunction $\Psi_0(t)$ of Eq. (9) is theoretically between $-\infty$ and $+\infty$ and not between $-T/2$ and $T/2$ like the Floquet eigenfunction, but both functions are similar after the same normalization.

Figure 8 shows the neutrally stable response $q(t)$ and modulation $V(t)$ at the tip of the second stability tongue of Fig. 8 for $T_\mathrm{O} = 0.21365$ s and $T_\mathrm{D}/T = 0.8$. The aforementioned properties remain for all tips of the stability tongues, so this new response is directly being visualized in the elementary time cell. Unlike the first synchronized stability mode in Figs. 4, 5, 6 and 7, the oscillating time $T_\mathrm{O}$ is longer and the mass is able to do two oscillations, i.e., $\dot{q}(t)$ is changing sign twice, before time reversing its dynamical state at the end of the impulsion. This mode of stabilization is associated with an asymmetric Floquet eigenfunction $\Psi(t)$ in the elementary time cell when the first mode described in Figs. 4, 5, 6 and 7 was symmetric. Again, upon the right scaling factors, it is possible to collapse the trajectories $q(t)$ of the tip of the second stability tongue to their Floquet eigenfunction as shown in Fig. 8b along with its associated modulation function $V(t)$. Taking $T_\mathrm{O} = 0.21365$ s and $\Delta V = 4.28$ mJ in the eigenvalue problem of Eq. (9), we find an eigenvalue $E_1 = 3.24$ mJ and an eigenfunction $\Psi_1(t)$ that indeed correspond to the results, we obtained from the original Initial Value Problem as shown in Fig. 8b. Unlike the previous case at the tip of the first stability tongue, $E_1$ and $\Psi_1(t)$ are the second eigenvalues and eigenfunctions of Eq. (9).

In the next section, we will generalize our approach to the whole space of the square-wave modulation functions $V(t)$ in order to rationalize the synchronized dynamical stabilization of our P.O.D.S.

## 4 Master curves for the stability tongues

### 4.1 From an initial value problem to a boundary value problem

Using the boundary conditions $\Psi(-\infty) = \Psi(+\infty) = 0$ and the matching conditions between the differentiable solutions of Eq. (9) inside and outside the well in the elementary time cell, one can establish two explicit continuity conditions, for symmetric and antisymmetric solutions $\Psi(t)$, that relate $E$, $T_\mathrm{O}$ and $\Delta V$ (Appendix 3 or [13]). Those continuity conditions cannot be satisfied for an arbitrary value of $E$. In the case of finite $\Delta V$ with $E < \Delta V$, i.e., for $V_\mathrm{D} < 0$ which is the framework of P.O.D.S., the "energy levels" $E_i$, eigenvalues of Eq. (9), and associated "bound states" $\Psi_i(t)$, eigenfunctions of Eq. (9), are discrete. Interestingly, there always exists at least one couple $(E_0, \Psi_0(t))$ even if the time well $\mathcal{U}(t)$ is very shallow.

By normalizing the potential height $\Delta V$ and energy levels $E$ by $8T_\mathrm{O}^2/I$, the normalized quantities

$$\Delta\tilde{V} = \Delta V \frac{8}{I} T_\mathrm{O}^2 \quad \text{and} \quad \tilde{E} = E \frac{8}{I} T_\mathrm{O}^2 \tag{10}$$

are giving explicitly the relation between the allowed triplets $(\Delta V, E, T_\mathrm{O})$ as

$$\Delta\tilde{V} = \frac{\sqrt{\tilde{E}}}{|\cos(\sqrt{\tilde{E}}/4)|} \quad \text{and} \quad \Delta\tilde{V} = \frac{\sqrt{\tilde{E}}}{|\sin(\sqrt{\tilde{E}}/4)|} \tag{11}$$

for symmetric and antisymmetric bound states, respectively. Those explicit master curves are shown in Fig. 9a in black and orange lines for symmetric and antisymmetric solutions, respectively. Each point on those curves represents an eigenvalue $E_i$ for a given potential





Journal: 11071 MS: 8501 TYPESET DISK LE CP Disp.:2023/5/16 Pages: 19 Layout: Medium

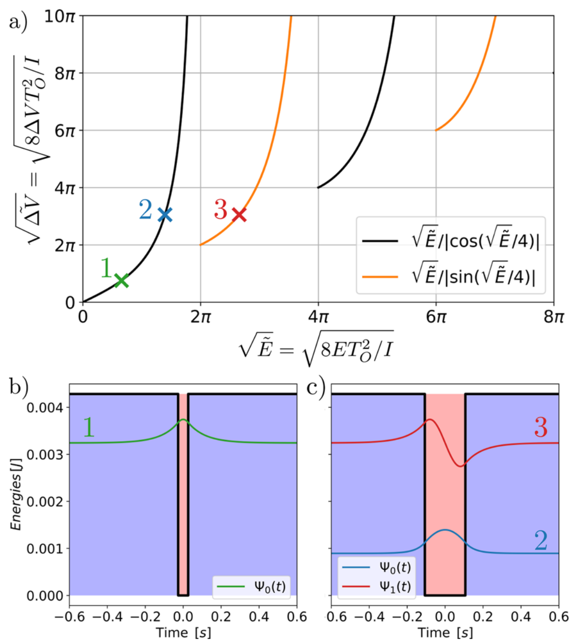


**Fig. 9** Energy levels of a particle in a finite potential well. **a** Possible values of $(\Delta V, E)$ for a mass with moment of inertia $I$ and energy $E \leq \Delta V$ in a potential well of depth $\Delta V$ and width $T_{\rm O}$. **b** Eigenvalue $E_0$ and eigenfunction $\Psi_0(t)$ for a finite well $\mathcal{U}(t)$ with height $\Delta V = 4.28$ mJ and width $T_{\rm O} = 0.052794$ s. **c** A finite potential well $\mathcal{U}(t)$ with height $\Delta V = 4.28$ mJ and width $T_{\rm O} = 0.21365$ s has two “bound states” $(E_0, \Psi_0(t))$ and $(E_1, \Psi_1(t))$

$\mathcal{U}(t)$ (defined by a couple $(\Delta V, T_{\rm O})$) in Eq. (9). Those eigenvalues are associated with an eigenfunction $\Psi_i(t)$ that read

$$\begin{cases} \Psi_i(t) = Ge^{\sigma t} \quad \text{for } t < -\dfrac{T_{\rm O}}{2} \\ \Psi_i(t) = A\cos(\omega t) + B\sin(\omega t) \quad \text{for} |t| \leq \dfrac{T_{\rm O}}{2} \\ \Psi_i(t) = He^{-\sigma t} \quad \text{for } t > \dfrac{T_{\rm O}}{2} \end{cases} \tag{12}$$

where $\sigma = \sqrt{\Delta\tilde{V} - \tilde{E}}/2T_{\rm O}$ and $\omega = \sqrt{\tilde{E}}/2T_{\rm O}$ are the local diverging and oscillating time scale of the mass, respectively. For the symmetric mode, we have $A = 0$ and $G = H$ when for the antisymmetric ones we impose $B = 0$ and $G = -H$. The eigenfunctions $\Psi_i(t)$ have to be continuous between $-\infty$ and $\infty$ so that the constants are fully defined once $\Psi(t)$ is normalized.

Figure 9b and c shows the classic “quantum” representation of the energy levels and bound states of a particle confined in a finite (or square-wave) potential well. It consists first of representing the potential $\mathcal{U}(t)$ (in black in Fig. 9b, c) with a red area for $|t| < T_{\rm O}/2$ where $E_i > \mathcal{U}(t)$ and blue areas for $|t| > T_O/2$ where $E_i < \mathcal{U}(t)$. On top of this potential $\mathcal{U}(t)$, we show the allowed bound states $(E_i, \Psi_i(t))$ where the origin of the local $y$-axis of the plotted $\Psi_i(t)$ coincides with the associated energy levels $E_i$.

A horizontal line in the master curves of Fig. 9a corresponds to a constant $\Delta\tilde{V}$, i.e., a given $\mathcal{U}(t)$. If $0 \leq \sqrt{\Delta\tilde{V}} < 2\pi$, only one bound state is allowed. This is the case of Fig. 9b (represented by a green cross in Fig. 9a where we fixed $I = mL^2 = 0.1076$ g m$^2$, $T_{\rm O} = 0.052794$ s and $\Delta V = 4.28$ mJ. The bound state $(E_0, \Psi_o(t))$ shown in Fig. 9b is the one we reported in Fig. 7 that allowed us to predict the modulation function $V(t)$ and the Floquet eigenfunction at the tip of the first instability tongue. For $2\pi \leq \sqrt{\Delta\tilde{V}} < 4\pi$, two bound states are allowed. This is for example the case of Fig. 9c (represented by a blue and red cross in Fig. 9a where we took $T_{\rm O} = 0.21365$ s this time. The second eigenmode $(E_1, \Psi_1(t))$ that is shown in red in Fig. 9c) is the one we reported in Fig. 8 that allowed us to predict the modulation function and the Floquet carrier of the response at the tip of the second stability region.

Interestingly, we see that this potential $\mathcal{U}(t)$ has a fundamental bound state $(E_0 = 0.895$ mJ, $\Psi_0(t))$, shown in blue line in Fig. 9c). Following our previous assumptions, it means that for a long diverging time $T_{\rm D} \gg T_{\rm O}$, the modulation function $V(t)$ with $\Delta V = 4.28$ mJ and $T_{\rm O} = 0.21365$ s should be able to dynamically stabilize the mass not only for $E_1 = 3.24$ mJ as in Fig, 8 but also for $E_0 = 0.895$ mJ. And the Floquet eigenfunction of the associated neutrally stable response should approximate $\Psi_0(t)$. This is indeed what we observe in Fig. 16 (Appendix 4). The mathematical problem of a particle in a finite potential well, summarized in the Liouville equation (9), is therefore a very good design tool to predict the modulation function that would stabilize the mass of the P.O.D.S governed by Eqs. (5)–(7) in the limit where $T_{\rm D} \gg T_{\rm O}$.

We recall we have dropped the time scale $T$ (or $T_{\rm D}$) in Eq. (8) to use Eq. (9) that has analytical solutions shown in Fig. 9. In the next subsection, we study the relevance of the analytical master curves of Fig. 9 in the original time-periodic Initial Value Problem Eqs. (5)–(7) where $T$ is present.





Journal: 11071 MS: 8501 TYPESET DISK LE CP Disp.:2023/5/16 Pages: 19 Layout: Medium

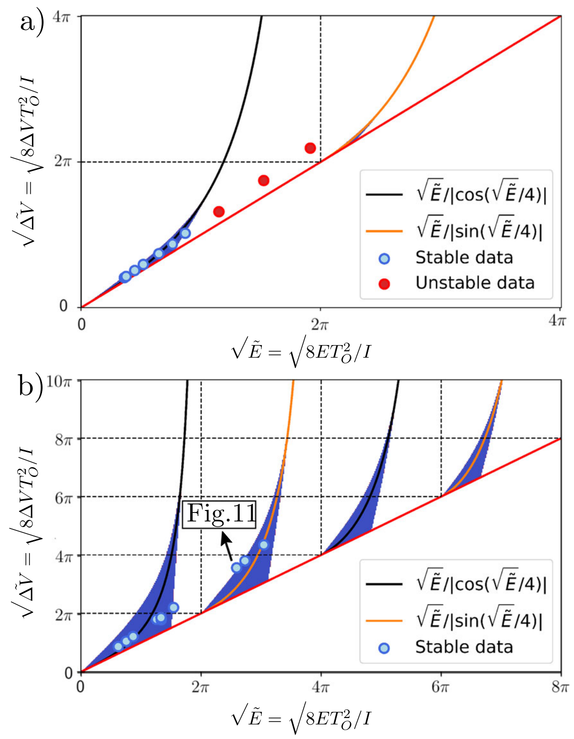


**Fig. 10** Stability diagram of the trivial state $(q(t), \dot{q}(t)) = (0, 0)$ of the square-wave P.O.D.S. governed by Eqs. (5)–(7) in the dimensionless $(\Delta\tilde{V}, \tilde{E})$ space. Blue regions indicate that a basin of attraction exist for which the mass is neutrally stable about (0, 0) when white regions show an unstable trivial state. Black and orange lines are the symmetric and antisymmetric master curves from the Liouville eigenproblem in Eq. (9) where we assumed $T_D \to T$ with $T = T_O + T_D$. The red line is the limit $E = \Delta V$, i.e., $V_D = 0$. Blue and red circles represent stable and unstable experimental data points, respectively. **a** $T_D/T = 0.7$. **b** $T_D/T = 0.25$

## 4.2 Finite diverging time $T_D$ and experimental validation

To continue rationalizing the stability behavior of the trivial fixed point $(q(t), \dot{q}(t)) = (0, 0)$ of the square-well P.O.D.S. we introduced in Sect. 2, we compute the stability diagram of the dynamical system given in Eqs. (5)–(7) in the dimensionless space $(\sqrt{\tilde{E}}, \sqrt{\Delta\tilde{V}})$ of Fig. 9a. The difference now with the Sturm–Liouville problem given in Eq. (9) is that the diverging time $T_D$ (and so the periodicity $T$) does exist in the original time-periodic system. For practical purposes, we simply need to analytically calculate the Floquet exponents on a given period of the Meissner equation Eq. (7). Inspired by the previous section, working in the periodic cell $-T/2 < t < T/2$, where we recall the period $T$ is the sum of the Oscillating and Diverging time such that $T = T_O + T_D$, and introducing the dimensionless time $\tau = 2t/T_O$, Eq. (7) can be recast in the dimensionless form

$$\begin{cases} \ddot{q}(\tau) + \dfrac{\tilde{E}}{16} q(\tau) = 0 & \text{for } |\tau| < 1 \\ \ddot{q}(\tau) - \dfrac{\Delta\tilde{V} - \tilde{E}}{16} q(\tau) = 0 & \text{for } 1 < |\tau| < T/T_O \end{cases} \tag{13}$$

where $\dot{()}$ now means derivative with respect to dimensionless time $\tau$. The normalized energies $\Delta\tilde{V}$ and $\tilde{E}$ are already introduced in Eq. (10). Figure 10a, b shows in blue regions, for $T_O/T = 0.3$ ($T_D/T = 0.7$) and $T_O/T = 0.75$ ($T_D/T = 0.25$), respectively, the couples $(\Delta\tilde{V}, \tilde{E})$ for which the real part of the two Floquet exponents is equal to zero, i.e., the mass is oscillating about $(q(t), \dot{q}(t)) = (0, 0)$ and therefore, there exists a basin of attraction for which $(q(t), \dot{q}(t)) = (0, 0)$ is dynamically stable in the nonlinear equation of motion Eq. (5). Interestingly, we see that the master curves previously defined in Eq. (9) for $0 < E < \Delta V$ are indeed a good approximation of the stability tongues of the P.O.D.S. when $T_D/T \to 1$ and $V_D < 0$ (the part of the stability tongues where $V_D > 0$ or $E > \Delta V$ is given in Fig. 17, Appendix 5).

Moreover, it turns out these master curves are inside the stability tongues whatever $T_D/T$ when $0 < E < \Delta V$, i.e., the master curves correspond to the only triplets $(T_O, \Delta V, E)$ that theoretically lead to a dynamically stable $(q(t), \dot{q}(t)) = (0, 0)$ whatever the period $T$. In practice, it means one just needs to fix $\Delta V$, $E$ and $T_O$ according to Eq. (11) in the square-wave modulation function $V(t)$ described in Fig. 1 to theoretically assure that the mass will be stable. From there, the more the diverging time $T_D$, the smaller the width of the tongue and basin of attraction, so the harder it is to actually stabilize the mass. Another interesting result is that the total number $N$ of possible stability tongues for a given $\Delta\tilde{V} = 8\Delta V T_O^2/I$ is simply determined by the floor function

$$N = \left\lfloor \frac{\sqrt{\Delta\tilde{V}}}{2\pi} \right\rfloor + 1 \tag{14}$$

which is a very useful design law for synchronized dynamical stabilization. Also, in the case of an infinite well, i.e., $\Delta V \to +\infty$, we have the simple result

$$\sqrt{\tilde{E}_i} \to 2\pi i \tag{15}$$

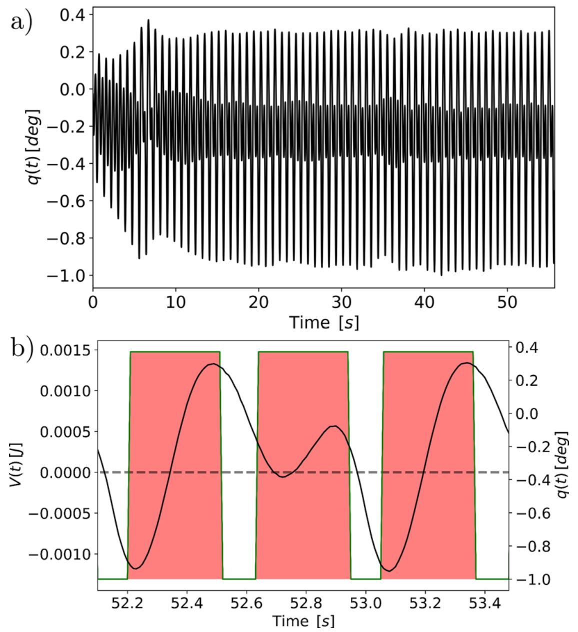


**Fig. 11** Experimental response and modulation function for $T_O = 309$ ms, $T_D/T = 0.25$, $E = 14.8$ mJ and $\Delta V = 2.8$ mJ (the experimental point is indicated in the $(\sqrt{\tilde{E}}, \sqrt{\Delta\tilde{V}})$ space in Fig. 10b. **a** Angular response of the inverted pendulum against time. **b** Zoom on three periods showing the modulation function $V(t)$ as well as the angular response as a function of time

as can be inferred from Fig. 10b.

In order to validate the design opportunity offered by the master curves of Fig. 10, we populate the stability diagram with experimental data points (in blue and red circles) from our electromagnetic inverted pendulum presented in Fig. 2. Because in our experiments, $I = mL^2 = 0.1076$ g.m$^2$ and $V_D = -\frac{1}{2} I\omega(0)^2 = -1.04$ mJ are fixed, and $E = \frac{1}{2} I\omega(i)^2$ and $\Delta V = E - V_D$ are barely controllable because $\omega(i)$ can only be varied between 18 rad/s and 33 rad/s as illustrated in Fig. 2, the main control that remains is the oscillating time $T_O$ which allow us to navigate along constrained slopes in the $(\Delta\tilde{V}, \tilde{E})$ space. By fixing $T_D/T = 0.7$ and the maximum authorized current $i = 0.55$ A (i.e., $\omega(i) \approx 33$ rad/s), we are able to populate Fig. 10a along a constant slope that is the minimal slope we can do in the $(\Delta\tilde{V}, \tilde{E})$ with this setup. We see that as soon as the experimental couple $(\Delta\tilde{V}, \tilde{E})$ is close to the first master curve $\Delta\tilde{V} = \sqrt{\tilde{E}}/|\cos(\sqrt{\tilde{E}}/4)|$ for $0 < \sqrt{\tilde{E}} < 2\pi$, the inverted pendulum is dynamically stabilized. When one moves away from this curve, the electromagnetic inverted pendulum is unstable. So the master curves are indeed a very good analytical warm start to dynamically stabilize a naturally diverging equilibrium in a synchronized fashion. Note that we were unable to observe the second stability region for $T_D/T = 0.7$, certainly because the width of the stability tongue, and therefore, the size of the basin of attraction was already too small.

To observe this second stability region, we needed to reduce the diverging time. In Fig. 10b, we plot in blue circle some stable experimental data points for various $T_O$, a fixed $T_D/T = 0.25$ and a minimal current $i = 0.4$ A so that the inverted pendulum is oscillating with a minimal frequency $\omega(i) = 16$ rad/s according to Fig. 2 (it is the highest slope we can do in the $(\Delta\tilde{V}, \tilde{E})$ space). Again, the inverted pendulum is dynamically stabilized when we are close to the master curves. Because $T_D/T$ is smaller than in Fig. 10a, the width of the stability region (and the size of the basin of attraction about $(q(t), \dot{q}(t)) = (0, 0)$) is larger and it is therefore easier to stabilize the system in a synchronized fashion. An experimental example of a synchronized stabilization in mode 2 is shown in Fig. 11 for a set of parameters indicated in the $(\sqrt{\tilde{E}}, \sqrt{\Delta\tilde{V}})$ space of Fig. 10b. We consider the electromagnetic pendulum is stabilized because, as shown in Fig 11a, even after 132 periods of modulation, the angular response of the pendulum does not exceed 1 degree which can be considered as experimental noise. Figure 11b shows a zoom on three periods as well as the experimental modulation function $V(t)$ that we considered to visualize when the electromagnets are ON leading to a positive $V(t)$ (this corresponds to the red regions). Given that $T_D/T = 0.25$, we are far from the tip of the stability regions and the experimental response does not yet resemble the second stationary bound state of a particle in a finite potential well. However, we recognize a second mode because of the anti-symmetric shape and the fact that the response is having two stationary points per period.

## 5 Conclusions

In this article, we have studied the local stability of a mass in a potential whose local curvature varies with time in a square wave fashion between a negative and positive value. This is a fundamental model to understand dynamical stabilization, which is a well-known concept in physics that notably explains the stabilization of an inverted pendulum in a local electromagnetic





Journal: 11071 MS: 8501 TYPESET DISK LE CP Disp.:2023/5/16 Pages: 19 Layout: Medium

field that we experimentally studied. We showed that stabilization “à la Kapitza”, at the heart of Floquet engineering in solid-state physics, that consists in applying a modulation time scale much faster than the natural time scales of the modulated system, is not the only way to dynamically stabilize the mass. An alternative is to stabilize in a “synchronized” fashion by periodically injecting the right amount of potential energy during the right time, i.e., the right elementary action. Doing so, one should be able to let the mass diverges for a relatively important time, i.e., minimize the total potential action required to dynamically stabilize a diverging mass. Interestingly, the Initial Value Problem inherent to this fundamental stability problem is related to the Boundary Value Problem underlying the determination of bound states and energy levels of a particle in a finite potential well, a famous problem in quantum mechanics. This analogy offers a semi-analytical design tool for the evaluation of the discrete set of piecewise constant modulation functions that will “optimally” stabilize the mass. Those results are also corroborated by numerical and experimental examples.

This work presents new physical insights on the concept of dynamical stabilization and uncovers a new class of dynamical systems similar in spirit to the time-crystals dynamics [19]. We have shown a way to discretize the set of periodic modulation functions allowed to dynamically stabilize the equilibrium of a time-periodic system. According to the mathematics of second-order differential equations with periodic coefficients [20,21], one should be able to discretize this set, not only by modulating a stiffness force, or the local curvature of the potential energy, as it was shown in this article, but also by modulating viscous forces in a way that still needs to be determined.

We focused here on a 1 degree of freedom P.O.D.S. with a square wave periodic modulation function. We should next investigate whether the aforementioned fundamental results could be generalized with more degrees of freedom and other modulation functions (some numerical results qualitatively similar to the one described in this article have been already seen on a P.O.D.S with a harmonic modulation function [8]). The theoretical argument in this study is mainly apprehended using a numerical and experimental approach. We believe a rigorous theoretical framework such as optimal control theory [22] could help in a near future to rationalize the intimate mathematical relation that seems to exist between the “optimal” dynamical stabilization of a naturally diverging mass in a time-periodic potential energy landscape, modeled by an initial value problem, and the physics of a particle confined in finite potential wells, that can be treated as a boundary value problem. Notably, investigating whether other mathematical features of the stationary Schrödinger equation such as superposition, quantum tunneling or entanglement could have some interpretations in the dynamics of P.O.D.S. would be useful to gain a deeper understanding of quantum analogs [23,24].

**Funding** A. Lazarus and S. Protière are grateful for financial support from Sorbonne University, France (EMERGENCES grants).

**Data availability** All numerical data in this work have been generated from the considered system equations Eqs.(1)–(14), with the approaches described in this work and the cited works, using Python. Therefore, it is possible to completely reproduce the data from the information given in this work.

**Declarations**

**Conflict of interest** The authors certify that they have no affiliations with or involvement in any organization or entity with any financial interest, or non-financial interest, in the subject matter or materials discussed in this manuscript.

## Appendix 1: Experimental P.O.D.S

In this appendix, we present in detail the experimental P.O.D.S built in the laboratory. In Fig. 12a, the metallic marble has a mass $m = 28$ g that is attached to a plexiglass rod of length $L = 6.2$ cm. The rod is then connected to another rod allowing it to rotate only in one plane. The marble is centered below the electromagnet (with typical holding force of 1000 N). Thanks to a Controllino card, we can turn ON and OFF the electromagnet in a very controlled and accurate manner in time. For the recording of the experimental responses, we place the electromagnetic inverted pendulum in front of a white LED to enhance the contrast and record the motion of the metallic marble with a Basler camera CMOS with 150 frames per second. The electromagnet is connected to a generator where we can select the value of the electrical current $i$. The electrical current is responsible of the intensity of the electromagnetic force near the inverted pendulum. The stronger the value of $i$, the stronger the electromagnetic field. By turning ON the electromagnet, the electromagnetic force will modify the effective gravitational





Journal: **11071** MS: **8501** TYPESET DISK LE CP Disp.:**2023/5/16** Pages: **19** Layout: **Medium**

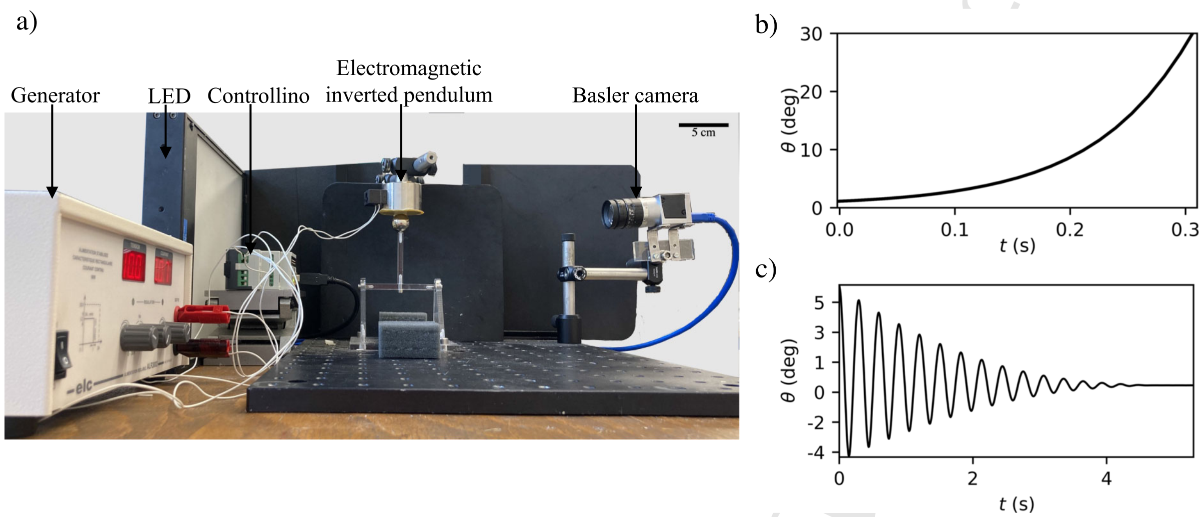


**Fig. 12** Electromagnetic inverted pendulum. **a** Planar inverted pendulum of length L with a metallic marble that is symmetrically placed under an attracting electromagnet whose attracting force depends on the imposed electrical current $i$. Experimental responses of the inverted electromagnetic pendulum for different values of the control parameter $i$. **b** $i = 0$ A: diverging response characterized by the natural frequency $\omega(0)$ **c** $i = 0.48$ A: damped oscillations about $\theta(t) \approx 0$ characterized by $\omega(0.48)$

field near the inverted pendulum, directly affecting the natural time scale of the inverted pendulum. To highlight this, the response for $i = 0$ and $i = 0.48$ A is shown in Fig. 12b, c, respectively. The natural response in Fig. 12b for $i = 0$ is a diverging one with a natural time scale to be $1/\omega(0) = 0.09$ s obtained by fitting an exponential function to the response. For $i = 0.48$ A, the response is damped oscillations about $\theta(t) \approx 0$ characterized by a natural frequency $\omega(0.48) = 19.5$ rad/s obtained by doing a Fast Fourier Transformation of the oscillatory response.

## Appendix 2: Influence of damping

In this appendix, we look at the influence of viscous damping on the stability diagram of Fig. 3. For practical purposes, we add a reduced damping term $\xi$ in Eq. (7) so that the linearized equation of motion about the trivial fixed point $(q(t), \dot{q}(t)) = (0, 0)$ is now

$$\begin{cases} \ddot{q}(t) + 2\xi\sqrt{\dfrac{2E}{I}}\dot{q}(t) + \dfrac{2E}{I}q(t) = 0 & \text{during } T_{\mathrm{O}} \\ \ddot{q}(t) + \dfrac{2V_{\mathrm{D}}}{I}q(t) = 0 & \text{during } T_{\mathrm{D}} \end{cases} \tag{16}$$

on a given period $T = T_{\mathrm{D}} + T_{\mathrm{O}}$, with $I = mL^2 = 1.076 \times 10^{-4}$ kg.m$^2$, $V_{\mathrm{D}} = -\frac{1}{2}I\omega(0)^2 = -1.04$ mJ and $E = V_{\mathrm{D}} + \Delta V = \frac{1}{2}I\omega(0.48)^2 = 3.24$ mJ. The stability diagram in the modulation parameter space $(T_{\mathrm{O}}, T_{\mathrm{D}})$ is given in Fig. 13 where the influence of damping is shown in pink regions (here $\xi = 0.05$). The influence of viscous damping is a well-known narrowing of the tip of the instability tongues. Interestingly, the tip of the stability tongues does not disappear when viscous damping is added. Although Eq. (16) seems more accurate than the undamped version Eq. (7) that we use in this article because our electromagnetic pendulum is indeed damped during $T_{\mathrm{O}}$, the undamped stability diagram seems in better agreement with our experimental data.

The thing is that there is a paradox when trying to predict the stable motions of the electromagnetic pendulum governed by the damped time-periodic Eq. (16). The upright electromagnetic pendulum is indeed doing damped oscillations when the electromagnets are ON and is diverging when the electromagnets are OFF. But if the electromagnets are turned ON during $T_{\mathrm{O}}$ and OFF during $T_{\mathrm{D}}$ in a piecewise constant periodic fashion, Eq. (16) will always predict that $q(t) \to 0$ when $t \to \infty$ in the case of stable couples $(T_{\mathrm{O}}, T_{\mathrm{D}})$. However, in the experiment, the upright pendulum will always oscillate with a finite amplitude even for very long time, because although damped during $T_{\mathrm{O}}$, the latter is periodically diverging during $T_{\mathrm{D}}$ so the slightest

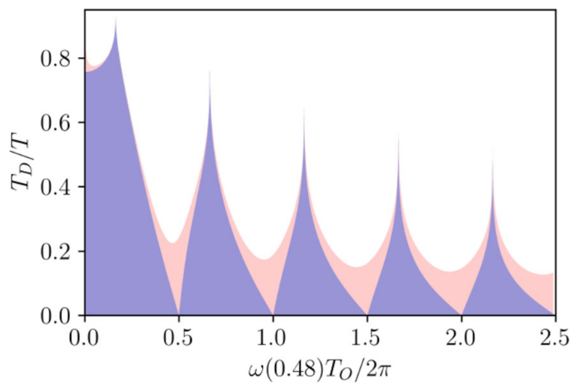


**Fig. 13** Numerical stability diagrams of the upright vertical electromagnetic pendulum governed by Eq. (16) when the current $i(t)$ is modulated with a piecewise constant $T$-periodic function. During $T_D$, $i = 0$ and the upright pendulum is diverging with a natural time scale $1/\omega(0)$ where $\omega(0) = 11.1$ rad/s. During $T_O$, $i = 0.48$ A and the pendulum is oscillating with a natural frequency $\omega(0.48) = 19.5$ rad/s. Blue regions represent dynamically stable $(T_O, T_D)$ for the damped ($\xi = 0.05$) and undamped ($\xi = 0$) scenario. Pink regions represent dynamically stable and unstable $(T_O, T_D)$ for the damped and undamped case, respectively. White regions represent unstable couple $(T_O, T_D)$ for both $\xi = 0$ and $\xi = 0.05$

imperfection that remains after the damped oscillations time $T_O$ will be amplified. A mass periodically doing damped oscillations and whose initial conditions are periodically "shuffled" by a diverging period is not correctly predicted by a time-periodic system like Eq. (16) and is maybe just difficult to predict at all because of the seemingly random nature of the symmetry breaking associated with the diverging time. This aspect, somehow similar to the so-called micro-chaotic oscillation of (mechanical) systems stabilized by digital control [25], could be interesting to investigate in a near future.

## Appendix 3: Particle in a finite potential well

To find the discrete energy levels $E$ for a mass under the effect of a finite square wave potential well of length $T_O$ and potential depth $\Delta V$ (Fig. 14) can be written as

$$\left(-\frac{I}{2}\frac{d^2}{dt^2} + \mathcal{U}(t)\right)\Psi(t) = E\Psi(t) \tag{17}$$

and $\Psi(-\infty) = \Psi(+\infty) = 0$, where $\Psi(t)$ is a wave function, $I$ is the moment of inertia of the mass and $\mathcal{U}(t)$ is the fixed square wave potential. Outside of the box $T_O$, the potential is $\Delta V$ and zero for $t$ between $-T_O/2$ and $T_O/2$. So, the wave function can be considered to be made up of different wave functions at different ranges of $t$, depending on whether $t$ is inside or outside of the box. Therefore, the wave function can be defined as:

$$\Psi(t) = \begin{cases} \Psi_1, \text{ if } t < -T_O/2 \\ \Psi_2, \text{ if } -T_O/2 < t < T_O/2 \\ \Psi_3, \text{ if } t > T_O/2 \end{cases} \tag{18}$$

### 5.1 Wave function inside the box

For the region inside the box, $\mathcal{U}(t) = 0$, Eq. (17) reduces to

$$-\frac{I}{2}\frac{d^2\Psi_2(t)}{dt^2} = E\Psi_2(t). \tag{19}$$

Equation (18) is a linear second-order differential equation with $E > 0$, so it has the general solution

$$\Psi_2(t) = A\sin(kt) + B\cos(kt) \tag{20}$$

where $k = \sqrt{2E/I}$ is a real number and $A$ and $B$ can be any complex numbers.

### 5.2 Wave function outside the box

For the region outside the box, $\mathcal{U}(t) = \Delta V$, Eq. (17) reduces to

$$-\frac{I}{2}\frac{d^2\Psi_1(t)}{dt^2} = (E - \Delta V)\Psi_1(t). \tag{21}$$

There are two possible families of solutions depending on whether $E$ is greater than $\Delta V$ (the particle is free) or $E$ is less than $\Delta V$ (the particle is bound in the potential).

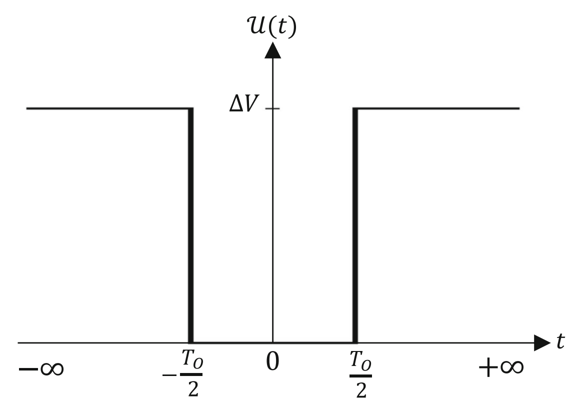


**Fig. 14** Finite square wave potential well of length $T_O$ and potential depth $\Delta V$





Journal: **11071** MS: **8501** TYPESET DISK LE CP Disp.:**2023/5/16** Pages: **19** Layout: **Medium**

In this analysis, we focus on the latter ($E < \Delta V$), so the general solution is an exponential of the shape

$$\Psi_1(t) = Fe^{-\alpha t} + Ge^{\alpha t}, \tag{22}$$

where $\alpha = \sqrt{2(\Delta V - E)/I}$ is a real number and $F$ and $G$ can be any complex numbers. Similarly, for the other region outside the box:

$$\Psi_3(x) = He^{-\alpha x} + Ie^{\alpha x}, \tag{23}$$

where $H$ and $I$ can be any complex numbers.

## 5.3 Wave function for the bound state

For the expression of $\Psi_1(t)$ in Eq. (22), we see that as $t$ goes to $-\infty$, the $F$ term goes to infinity. Likewise, in Eq. (23) as $t$ goes to $+\infty$, the $I$ term goes to infinity. In order for the wave function to be square integrable, we must set $F = I = 0$.

Next, we know that the overall $\Psi(t)$ function must be continuous and differentiable. These requirements are translated as boundary conditions on the differential equations previously derived. So, the values of the wave functions and their first derivatives must match up at the dividing points:

$$\begin{cases} \Psi_1(-T_O/2) = \Psi_2(-T_O/2),\ \Psi_2(T_O/2) = \Psi_3(T_O/2) \\ \dfrac{d\Psi_1}{dt}\Big|_{t=-\frac{T_O}{2}} = \dfrac{d\Psi_2}{dt}\Big|_{t=-\frac{T_O}{2}} \text{ and } \dfrac{d\Psi_2}{dt}\Big|_{t=\frac{T_O}{2}} = \dfrac{d\Psi_3}{dt}\Big|_{t=\frac{T_O}{2}} \end{cases}$$

giving the system of equations

$$\begin{cases} Ge^{-\alpha T_O/2} = -A\sin(kT_O/2) + B\cos(kT_O/2) \\ He^{-\alpha T_O/2} = A\sin(kT_O/2) + B\cos(kT_O/2) \\ \alpha Ge^{-\alpha T_O/2} = Bk\sin(kT_O/2) + Ak\cos(kT_O/2) \\ \alpha He^{-\alpha T_O/2} = Bk\sin(kT_O/2) - Ak\cos(kT_O/2) \end{cases} \tag{24}$$

Finally, the finite square-wave potential well is symmetric (Fig. 14), so symmetry can be exploited to reduce the necessary calculations. This means that the system in Eq. (24) has two sorts of solutions: symmetric and antisymmetric solutions.

### 5.3.1 *Symmetric solutions*

To have a symmetric solution, we need to impose $A = 0$ and $G = H$. Equation(24) reduces to

$$\begin{cases} He^{-\alpha T_O/2} = B\cos(kT_O/2) \\ \alpha He^{-\alpha T_O/2} = Bk\sin(kT_O/2) \end{cases}$$

and taking the ratio gives

$$\alpha = k\tan(kT_O/2), \tag{25}$$

which is the energy equation for the symmetric solutions.

### 5.3.2 *Antisymmetric solutions*

For the antisymmetric solutions, we need to have $B = 0$ and $G = -H$. Equation(24) reduces to

$$\begin{cases} He^{-\alpha T_O/2} = A\sin(kT_O/2) \\ -\alpha He^{-\alpha T_O/2} = Ak\cos(kT_O/2) \end{cases}$$

and taking the ratio gives

$$\alpha = -k\cot(kT_O/2) \tag{26}$$

which is the energy equation for the antisymmetric solutions.

### 5.3.3 *Master equations*

The energy equations (25, 26) cannot be solved analytically. Nevertheless, if we introduce the dimensionless variables $u = \alpha T_O/2$ and $v = kT_O/2$, we obtain the following master equations

$$\sqrt{u_0^2 - v^2} = \begin{cases} v\tan(v), & \text{symetric case} \\ -v\cot(v), & \text{antisymmetric case} \end{cases} \tag{27}$$

where $u_0^2 = \Delta V T_O^2/2I$ and $v^2 = ET_O^2/2I$. So, for a fixed square-wave potential $(\Delta V, T_O)$, the intersections $(v_i)$ solution of Eq. (27) let us infer the discrete energy levels $E_i = 2Iv_i^2/T_O^2$. Then, having the values of $E_i$ we can deduce the values of $\alpha_i$ and $k_i$ and infer the wave function $\Psi_i(t)$.

Figure 15 shows two examples of application for the master equations (27). In Fig. 15a, the potential barrier $\Delta V$ and the length of the box $T_O$ gives $u_0^2 = 5$. Then, by solving the master equations (27) we obtain two intersections points $(v_1, v_2)$. Then, we deduce the two discrete energy levels $E_{1,2}$ and the corresponding wave functions $\Psi_{1,2}(t)$ for this giving square-wave potential (represented in blue and green, respectively, in Fig. 15a). Figure.15b represents another example where $u_0^2 = 31.25$. The solution of the master equation (27) gives four intersection points. We deduce the discrete energy levels $E_{1,2,3,4}$ and the corresponding wave functions $\Psi_{1,2,2,4}(t)$ (represented in blue, green, orange and purple in Fig. 15b).





Journal: 11071 MS: 8501 TYPESET DISK LE CP Disp.:2023/5/16 Pages: 19 Layout: Medium

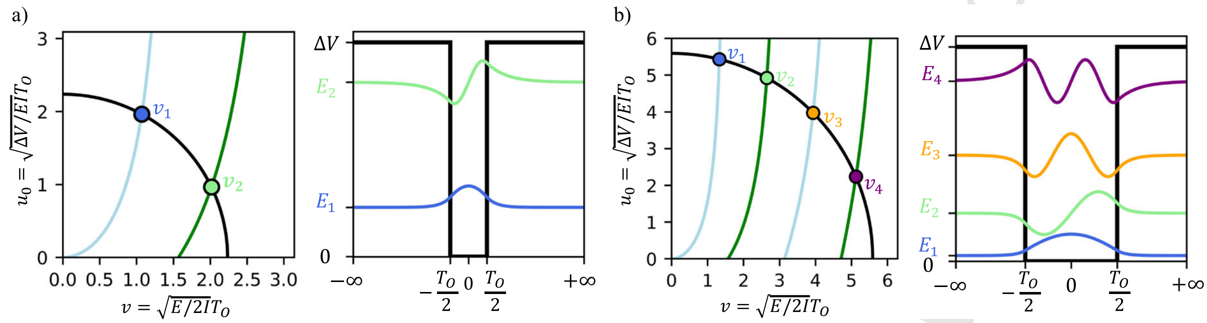


**Fig. 15** Master equations to deduce the discrete energy levels $E_i$ and the corresponding wave function $\Psi_i(t)$. **a** Square wave potential fixed at $u_0^2 = 5$ gives two intersection points of the master curves which translates into two energy levels $E_{1,2}$ and the corresponding wave function $\Psi_{1,2}(t)$ represented in blue and green. **b** Square wave potential fixed at $u_0^2 = 31.25$ gives four intersection points of the master curves which translate into four energy levels $E_{1,2,3,4}$ and the corresponding wave function $\Psi_{1,2,3,4}(t)$ represented in blue, green, orange and purple, respectively

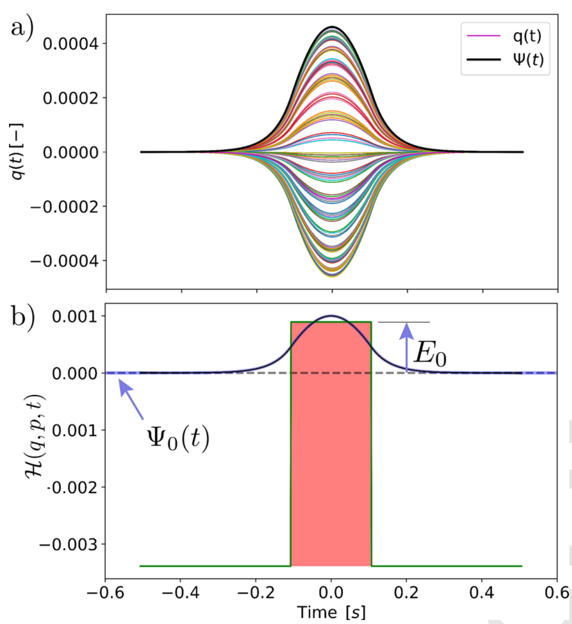


**Fig. 16** Neutrally stable response for $I = mL^2 = 0.1076$ g.m$^2$, $\Delta V = 4.28$ mJ, $E = 0.895$ mJ, $T_O = 0.21365$ s and $T_D = 0.8$ s visualized in the elementary time cell $-T/2 < t < T/2$ with $T = T_O + T_D$. **a** Evolution of the generalized coordinate $q(t)$ and Floquet eigenfunction $\Psi(t)$. **b** Collapse of the trajectories $q(t)$ of **a** on the Floquet eigenfunction $\Psi(t)$ and evolution of the associated modulation function $V(t)$ (equivalent to $\mathcal{H}(q, p, t)$). The eigenfunction $\Psi_0(t)$ and eigenvalue $E_0$ of Eq. (9) are reported on the figure

It is interesting to mention that the resolution previously showed is also the mathematical resolution of the classical problem of a particle trapped in a finite potential well in quantum mechanics [13,26].

## Appendix 4: Fundamental bound state for $T_O = 0.21365$ s

The resolution of the Liouville eigenvalue problem Eq. (9) suggested that for $I = 0.1076\,\text{g}\,\text{m}^2$, $\Delta V = 4.28$ mJ and $T_O = 0.21365$ s, a modulation function with $E = 0.895$ mJ would stabilize the mass even when the diverging time $T_D$ is large. This result is summarized in Fig. 9 that showed the "bound states" and "energy levels" of the particle confined in a finite potential well for $T_O = 0.21365$ s and $\Delta V = 4.28$ mJ. In Fig. 16, we show the response of the mass governed by the linear Initial Value Problem Eq. (7) when using the modulation function $V(t)$ suggested by the eigenvalue problem Eq. (9). In Fig. 16a, the 100th first periods of the dynamical response $q(t)$ are superposed in the elementary time cell $[-T/2, T/2]$ alongside with its Floquet eigenfunction $\Psi(t)$ shown in black thin line. As predicted by the Boundary Value Problem, the response is neutrally stable even if $T_D$ is large. Moreover, upon the correct scaling, one can collapse all the trajectories on a single curve in $[-T/2, T/2]$ that is the Floquet eigenfunction $\Psi(t)$ of the response as shown in Fig. 16b where we also plot the piecewise constant modulation function $V(t)$ (that is very close to the total energy of the mass) in green line. The eigenvalue and eigenfunction of Eq. (9) are also reported in this figure. As expected, they match with the outcome of our Initial Value Problem. The Boundary Value Problem Eq. (9) is therefore a good design tool to predict what modulation function will dynamically stabilize the mass even for a


Journal: 11071 MS: 8501 TYPESET DISK LE CP Disp.:2023/5/16 Pages: 19 Layout: Medium

long diverging time $T_D$ and what will be the qualitative shape of the oscillatory response over each period.

## Appendix 5: Extended stability diagram in the $(\sqrt{\bar{E}}, \sqrt{\Delta \bar{V}})$ space

In Fig. 10, we showed the linear stability diagram of our square-wave Periodically Oscillating Diverging System (P.O.D.S.) governed by the dimensionless equation Eq. (13) in the $(\sqrt{\bar{E}}, \sqrt{\Delta \bar{V}})$ space for $0 < E < \Delta V$, i.e., $V_D < 0$ that is the P.O.D.S. formalism. In Fig. 17, we show this stability diagram in the general case that allow $E > \Delta V$, i.e., $V_D > 0$ that is the case when the particle is in a potential whose local curvature varies between only positive values, in a square-wave fashion in our case. What we see in Fig. 17 is then the classic instability tongues (white regions) of the Meissner equation Eq. (13) that has been extensively studied in the literature [9,17,18,21].

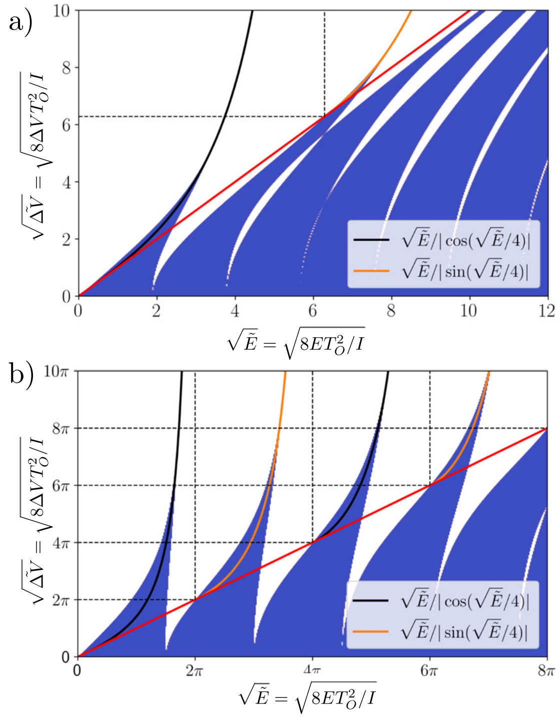


**Fig. 17** Stability diagram of the trivial state $(q(t), \dot{q}(t)) = (0, 0)$ of the square-wave P.O.D.S. governed by Eqs. (5)–(7) in the dimensionless $(\Delta\tilde{V}, \tilde{E})$ space. Blue regions indicate that a basin of attraction exist for which the mass is neutrally stable about $(0, 0)$ when white regions show an unstable trivial state. Black and orange lines are the symmetric and antisymmetric master curves from the Liouville eigenproblem in Eq. (9) where we assumed $T_D \to T$ with $T = T_O + T_D$ and $E < \Delta V$ (or $V_D < 0$). The red line is the limit $E = \Delta V$, i.e., $V_D = 0$. Below this red line, we have $V_D > 0$, the case of a particle in a potential energy with a time-varying local curvature that always remain positive. **a** $T_D/T = 0.7$. **b** $T_D/T = 0.25$

## References


1. Holtaus, M.: Floquet engineering with quasienergy bands of periodically driven optical lattices. J. Phys. B: At. Mol. Opt. Phys. **49**(1), 013001 (2015)
2. Oka, T., Kitamura, S.: Floquet engineering of quantum materials. Ann. Rev. Condens. Matter Phys. **10**(1), 387–408 (2019)
3. Smith, H.J.T., Blackburn, J.A.: Experimental study of an inverted pendulum. Am. J. Phys. **60**(10), 909–911 (1992)
4. Acheson, D.J.: Upside-down pendulums. Nature **366**, 215–216 (1993)
5. Apffel, B., Novkoski, F., Eddi, A., Fort, E.: Floating under a levitating liquid. Nature **585**(7823), 48–52 (2020)
6. Wolfgang, P.: Electromagnetic traps for charged and neutral particles. Rev. Mod. Phys. **62**(3), 531 (1990)
7. Chávez-Cervantes, M., Topp, G.E., Aeschlimann, S., Krause, R., Sato, S.A., Sentef, M.A., Gierz, I.: Charge density wave melting in one-dimensional wires with femtosecond subgap excitation. Phys. Rev. Lett. **123**(3), 036405 (2019)
8. Lazarus, A.: Discrete dynamical stabilization of a naturally diverging mass in a harmonically time-varying potential. Physica D **386–387**, 1–7 (2019)
9. Grandi, A.A., Protière, S., Lazarus, A.: Enhancing and controlling parametric instabilities in mechanical systems. Extreme Mech. Lett. **43**, 101195 (2021)
10. Bukov, M., D'Alessio, L., Polkovnikov, A.: Universal high-frequency behavior of periodically driven systems: from dynamical stabilization to floquet engineering. Adv. Phys. **64**(2), 139–226 (2015)
11. Stephenson, A.: XX. On induced stability. Lond. Edinb. Dublin Philos. Mag. J. Sci. **15**(86), 233–236 (1908)
12. Kapitza, P.L.: Dynamical stability of a pendulum when its point of suspension vibrates, and pendulum with a vibrating suspension. Collected Papers of PL Kapitza **2**, 714–737 (1965)
13. Messiah, A.: Quantum Mechanics, vol. 1. North-Holland, Province (1961)
14. Protière S., Grandi, A.A., Lazarus, A.: Movie 1 showing the natural diverging response of the electromagnetic inverted pendulum with a time scale of $1/\omega(0) = 0.09$s. *Movie 2* showing the experimental response of the electromagnetic inverted pendulum under a constant electromagnetic field for $i = 0.48$ A characterized by an angular frequency $\omega(i) = 19.5$ rad .s$^{-1}$
15. Calico, R.A., Wieself, W.E.: Control of time-periodic systems. J. Guid. Control. Dyn. **7**(6), 671–676 (1984)
16. Bentvelsen, B., Lazarus, A.: Modal and stability analysis of structures in periodic elastic states: application to the Ziegler column. Nonlinear Dyn. **91**(2), 1349–1370 (2018)






Journal: **11071** MS: **8501** TYPESET DISK LE CP Disp.:**2023/5/16** Pages: **19** Layout: **Medium**

17. van der Pol, B., Strutt, M.J.O.: II. On the stability of the solutions of Mathieu's equation. Lond. Edinb. Dublin Philos. Mag. J. Sci. **5**(27), 18–38 (1928)
18. Sato, C.: Correction of stability curves in Hill–Meissner's equation. Math. Comput. **20**(93), 98–106 (1966)
19. Shapere, A.D., Wilczek, F.: Regularizations of time-crystal dynamics. Proc. Natl. Acad. Sci. **116**(38), 18772–18776 (2019)
20. Magnus, W., Winkler, S.: Hill's Equation. Courier Corporation, New York (1966)
21. Richards, J.A.: Analysis of Periodically Time-Varying Systems. Springer, New York (2012)
22. Kirk, D.E.: Optimal Control Theory: An Introduction. Courier Corporation, New York (2004)
23. Perrard, S., Labousse, M., Miskin, M., Fort, E., Couder, Y.: Self-organization into quantized eigenstates of a classical wave-driven particle. Nat. Commun. **5**, 3219 (2014)
24. Bush, J.W.M.: Pilot-wave hydrodynamics. Ann. Rev. Fluid Mech. **47**, 269–292 (2015)
25. Haller, G., Stépán, G.: Micro-chaos in digital control. J. Nonlinear Sci. **6**(5), 415–448 (1996)
26. Griffiths, D., Schroeter, D.: Introduction to Quantum Mechanics. Pearson Prentice Hall, Upper Saddle River (2005)








Journal: **11071** MS: **8501** TYPESET DISK LE CP Disp.:**2023/5/16** Pages: **19** Layout: **Medium**